

CST Parametric Modeling and Multi-Objective Optimization Reconfiguration Study of a Blended-Wing-Body Aircraft

Xingquan Lu [1], Shusheng Chen[1], Xinghai Wang[1], Jiajia Yu[1] & Dong Li[1]

[1] School of Aeronautics, Northwestern Polytechnical University, Xi'an 710072, China

Contact Author:
Shusheng Chen, School of Aeronautics, Northwestern Polytechnical Univ., No. 127, Youyi West Rd., Xi'an, 710072, China. (Email: sshengchen@nwpu.edu.cn)

Abstract

The Blended-Wing-Body (BWB) aircraft has become a significant development direction for future civil and special-mission aircraft due to its superior lift-to-drag ratio and structural efficiency. However, its fuselage and inboard wing sections feature complex aerodynamic shapes and strong longitudinal coupling characteristics, posing challenges for aerodynamic design and performance optimization. Focusing on these sections, this paper proposes a multi-section airfoil optimization and reconstruction method based on CST parameterization, and constructs a comprehensive airfoil evaluation index to achieve synergistic optimization of lift-to-drag and pitching moment characteristics. First, characteristic sections of the fuselage and inboard wing are selected to generate multiple airfoils. Second, to collaboratively evaluate lift, drag, and pitching moment, a comprehensive index based on aerodynamic center transfer and statistical normalization is constructed to select the optimal airfoil. Finally, the optimized airfoils are assembled, and the topological design of the fuselage and inboard wing sections is carried out. Numerical simulation results show that under the design condition, the flow separation zone of the full BWB aircraft is reduced, while the lift-to-drag ratio increases by 4.72%, the drag coefficient decreases by 7.3%, and the inflection point position of the pitching moment curve is delayed by 15.44%. This method can improve the lift-to-drag characteristics while taking the moment characteristics into account and achieve a delayed pitching moment inflection point, providing a reference for the refined aerodynamic design of BWB aircraft.

Keywords: Blended-Wing-Body; CST parameterization; multi-section airfoil optimization; aerodynamic synergistic optimization; comprehensive performance index

1. Introduction

The Blended-Wing-Body (BWB) configuration achieves synergistic improvements in aerodynamic and structural efficiency through smooth blending of the fuselage and wing, and has become a significant development direction for future civil and special-mission aircraft [1,2]. However, while gaining lift-to-drag advantages, this configuration also introduces unique aerodynamic design challenges. The fuselage and inboard wing sections of a BWB feature complex blended shapes and strong three-dimensional flow characteristics, where flow separation is prone to occur at the swept-wing root, causing unfavorable inflection points in the pitching moment curve at certain angles of attack and directly threatening longitudinal handling and stability qualities [3,4].

Existing studies have conducted extensive aerodynamic analysis and optimization design work on BWB configurations. The BWB configuration combines high aerodynamic efficiency with environmental benefits and is suitable for integrating advanced technologies such as laminar flow control and distributed propulsion; yet its highly tightly coupled nature also presents severe multidisciplinary design challenges. Research has shown that HWB configurations can achieve 39%–54% fuel savings compared with conventional layouts, and over-body engines can significantly reduce noise and emissions [5,6].

https://doi.org/10.71945/icas2026_0455

The weight estimation bias of non-circular pressurized cabins, differences in transonic compressibility drag estimation, and the “unusable white space” empty weight penalty at small scales remain bottlenecks in accurate evaluation [7]. Wang et al. systematically reviewed the overall aerodynamic technical challenges and development prospects of BWB civil aircraft, pointing out that the technical bottlenecks lie in aerodynamic layout design principles and the coordination of high- and low-speed performance [8]. Ali et al. reviewed the latest advances in aerodynamic efficiency, stability, and control optimization of BWB configurations, emphasizing the core role of multidisciplinary optimization frameworks in overcoming the stability challenges of tailless aircraft [9,10]. In terms of numerical optimization, Rizzi et al. proposed a strategy of decomposing BWB aerodynamic design into two-dimensional airfoil design and three-dimensional twist optimization, achieving significant drag reduction benefits under constraints [11-13]. However, the above studies mostly focus on improving lift-to-drag characteristics at cruise conditions, without adequately addressing moment characteristics. In particular, active suppression strategies for the inflection point of the pitching moment curve have been seldom explored, which objectively restricts the improvement of longitudinal stability of BWB configurations across the entire flight envelope [14,15].

In the area of geometric modeling, the Class-Shape Transformation (CST) method proposed by Kulfan has been widely applied in aircraft shape parameterization due to its few parameters and strong shape-preserving capability [16]. Lane et al. extended the CST method to the parameterization of complex surfaces incorporating circulation control configurations, validating its feasibility in BWB configuration modeling [17]. In recent years, the CST method has also been employed in benchmark studies of airfoil parameterization and optimization, demonstrating its robustness and flexibility in complex design spaces [18,19]. The perturbation CST method, which superimposes CST-shaped geometric perturbations onto a baseline airfoil, can achieve a favorable balance between convergence and geometric rationality [20-22]. To further enhance the descriptive capability of CST, researchers have developed variants such as improved CST with leading-edge aerodynamic concerns [23], orthogonal CST [24], three-dimensional CST [25], and B-spline enhanced CST [26], providing richer tools for the refined modeling of complex blended shapes.

To address the above issues, this paper proposes a multi-section airfoil optimization and reconstruction method for the BWB fuselage and inboard wing sections based on perturbation CST parameterization. First, characteristic sections along the spanwise direction of the BWB blending region are selected, and a family of airfoils is generated using the perturbation CST method. Second, a dimensionless comprehensive performance index W_{01} is constructed based on aerodynamic center transfer and statistical normalization techniques to collaboratively evaluate lift, drag, and pitching moment about the aerodynamic center, thereby achieving a “three-in-one” optimization. Finally, the three-dimensional assembly of the optimized airfoils is accomplished through two-dimensional transformation and trailing-edge thickness adjustment, yielding a parametric geometric model of the BWB blending region. Numerical simulation results show that this method improves the cruise lift-to-drag ratio, reduces the absolute value of the pitching moment, and delays the pitching moment inflection point, thereby providing a feasible technical pathway for the refined aerodynamic design of BWB configurations.

2. CST Parametric Modeling and Multi-Section Airfoil Reconstruction

2.1 Basic CST Method

The CST method describes the geometric coordinates of an airfoil through the product of the class function $C(x)$ and the shape function $S(x)$. For the upper and lower surfaces of the airfoil, the expression is:

$$y_u(x) = C(x) \cdot S_u(x) + x \cdot y_{TEu} \tag{1}$$

$$y_l(x) = C(x) \cdot S_l(x) + x \cdot y_{TEl} \tag{2}$$

where the class function $C(x)$ is defined as:

$$C(x) = x^{N1} \cdot (1-x)^{N2} \tag{3}$$

For conventional airfoils, the exponents are taken as N_1=0.5, N_2=1.0. The shape function $S(x)$ is expanded using Bernstein polynomials:

$$S_u(x) = \sum_{i=0}^{N} A_{u_i} \cdot B_i(x) \tag{4}$$

$$S_l(x) = \sum_{i=0}^{N} A_{l_i} \cdot B_i(x) \tag{5}$$

The Bernstein polynomial $B_i(x)$ is defined as:

$$B_i(x) = \frac{N!}{i!(N-i)!} x^i (1-x)^{N-i}, \quad i = 0,1,\ldots,N \tag{6}$$

where A_{ui} and A_{li} are the undetermined coefficients, i.e., the design variables; N is the order of the Bernstein polynomial.

The figure below shows the CST fitting and fitting error for the typical airfoil AG 03 at different orders N. No obvious geometric errors are observed, and the maximum error is 0.4%, indicating that the CST method possesses good effectiveness and shape-preserving capability for airfoil fitting.

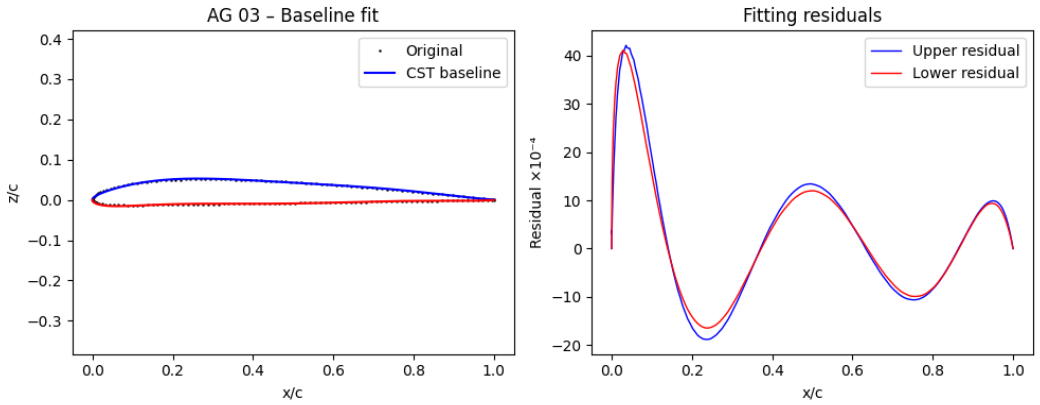


Figure 1 – Schematic of CST fitting and fitting error plot for the AG 03 airfoil（N=4）

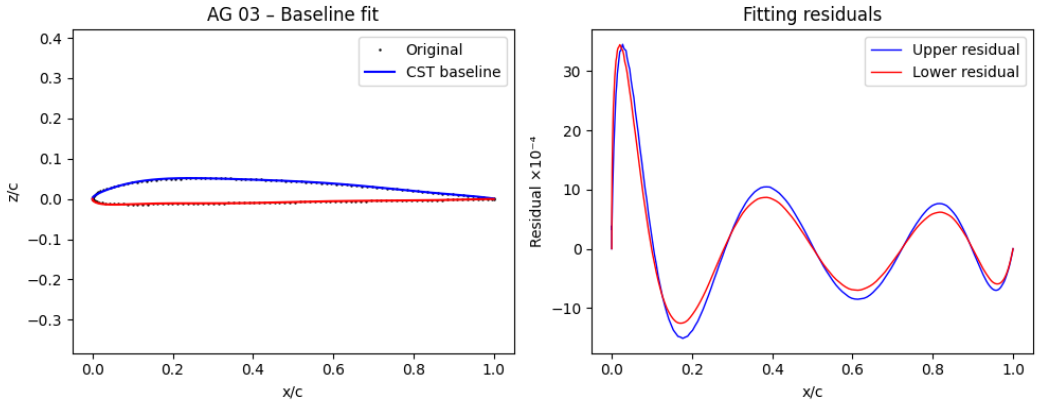


Figure 2 – Schematic of CST fitting and fitting error plot for the AG 03 airfoil（N=5）

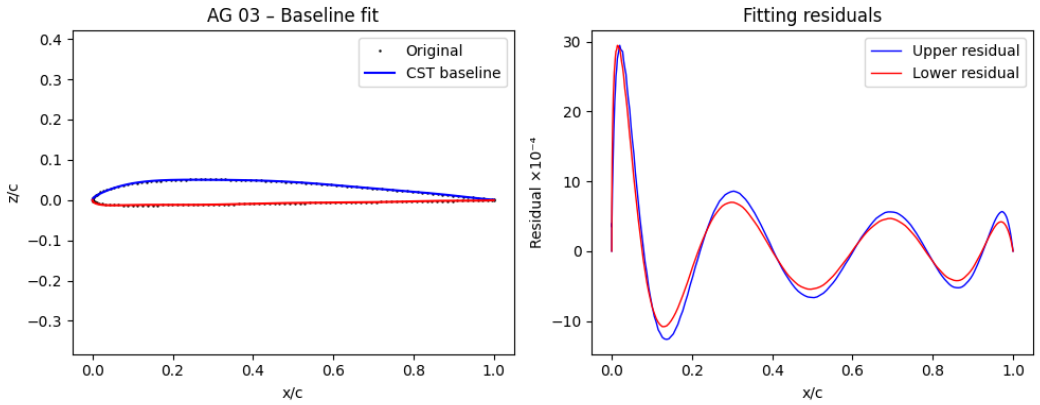


Figure 3 – Schematic of CST fitting and fitting error plot for the AG 03 airfoil（N=6）

For the fuselage and inboard wing sections of the BWB aircraft, k = 3 characteristic sections are selected: Section A (symmetry plane, y = 0 mm), Section B (fuselage section, y = 650 mm), and Section C (inboard wing section, y = 1200 mm). The baseline airfoil for each section is taken from the profile of the original BWB configuration at that spanwise location. Considering both fitting accuracy and the dimension of control variables, a 5th-order Bernstein polynomial is adopted for the CST fitting of the multi-section airfoils. The fitting accuracy for each airfoil is controlled within 0.7%, with 6 control variables for the upper surface and 6 for the lower surface, resulting in a total of 12 variables.

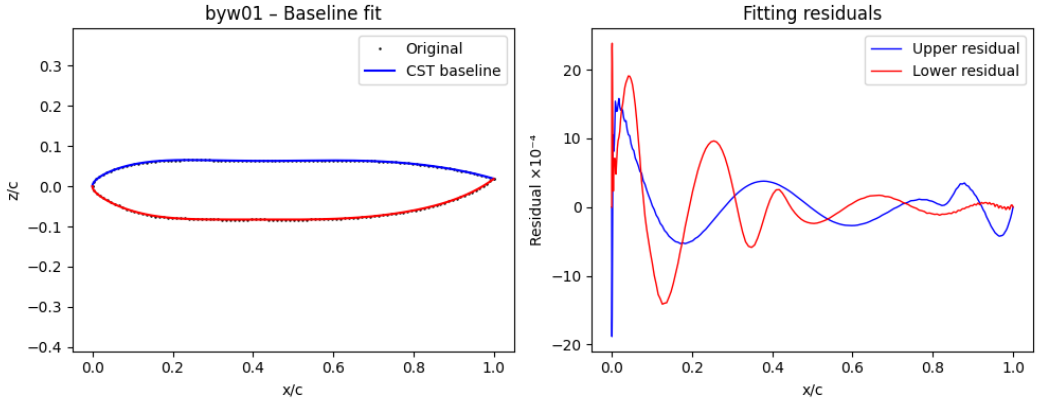


Figure 4 – Schematic of CST fitting and fitting error plot for the byw01 airfoil(N=5，y=0mm)

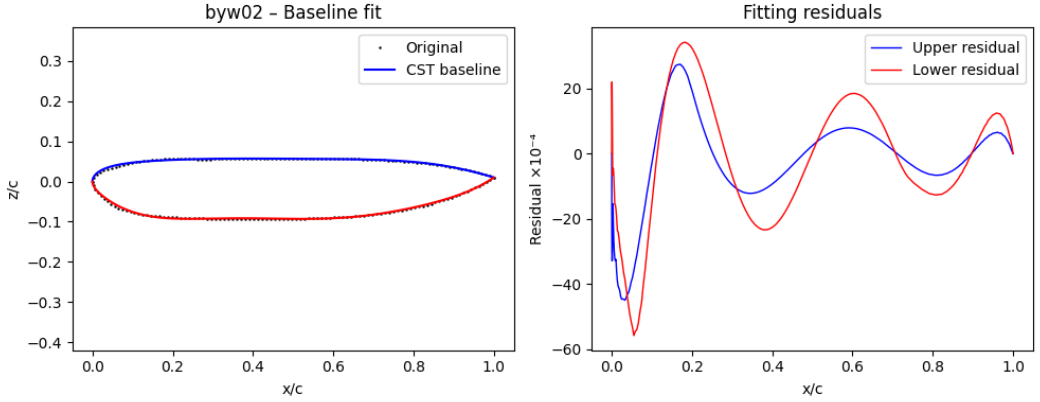


Figure 5 – Schematic of CST fitting and fitting error plot for the byw02 airfoil(N=5，y=650mm)

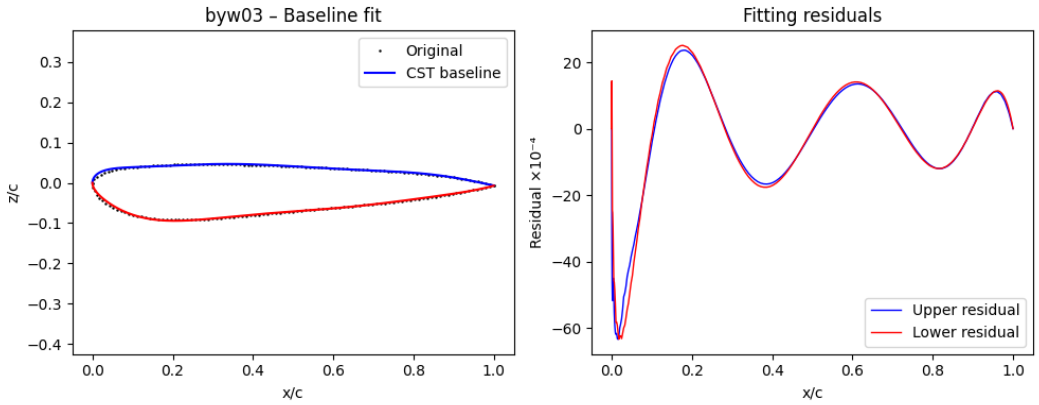


Figure 6 – Schematic of CST fitting and fitting error plot for the byw03 airfoil (N=5，y=1200mm）

2.2 Perturbation CST Method

The perturbation CST method generates a new airfoil by superimposing a geometric perturbation in CST form onto the coordinates of a baseline airfoil. The expression is:

$$y(x) = y_0(x) + x^{N1} \cdot (1-x)^{N2} \cdot \sum_{i=0}^{N} A_i x^i \tag{7}$$

where $y_0(x)$ is the ordinate of the baseline airfoil, and A_i are the perturbation coefficients (design variables).

This method is characterized by preserving the basic aerodynamic characteristics of the baseline airfoil while searching for a better shape only within a small range, offering better convergence and geometric rationality.

Each section is independently parameterized using the perturbation CST method, with the design variables being the perturbation coefficients A_i of that section. In this study, the Bernstein polynomial order $N = 5$ is adopted, resulting in $2(N+1) = 12$ design variables per section and a total of 36 design variables for the three sections. The range of each variable is $[-0.03, 0.03]$ to ensure a moderate perturbation amplitude that does not compromise the basic geometric features of the airfoil.

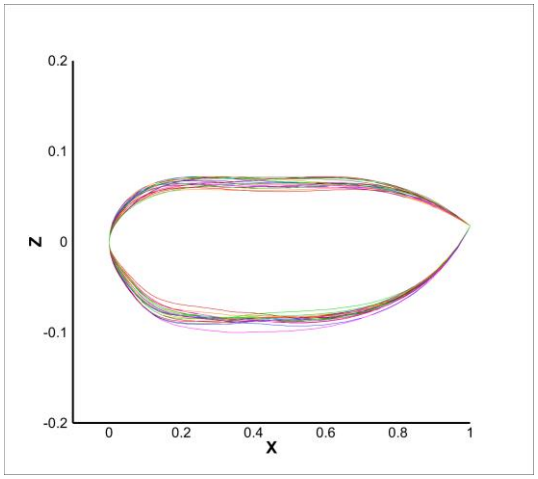


Figure 7 – byw01 Airfoil Family

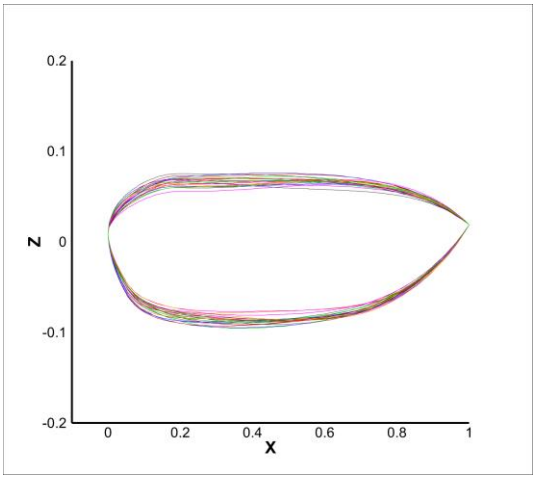


Figure 8 – byw02 Airfoil Family

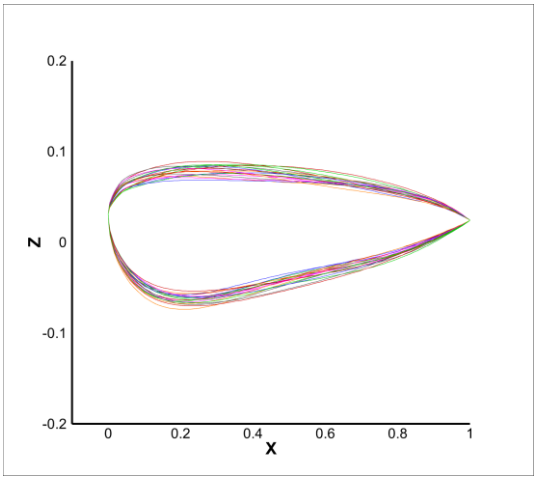


Figure 9 – byw03 Airfoil Family

3. Numerical Computation Method

3.1 Governing Flow Equations and Turbulence Model

This paper employs the Reynolds-Averaged Navier–Stokes (RANS) equations to numerically simulate the flow around the airfoil and the full aircraft. The integral form of the governing equations is:

$$\frac{\partial}{\partial t}\iiint_{\Omega}\mathbf{Q}d\Omega+\iint_{\partial\Omega}\left(\mathbf{F}_c-\mathbf{F}_v\right)\cdot\mathbf{n}dS=0 \tag{8}$$

where $\mathbf{Q}$ denotes the conservative variable, and $\mathbf{F}_c$ and $\mathbf{F}_v$ are the convective and viscous fluxes, respectively.

Turbulence modeling adopts the Spalart–Allmaras (S–A) one-equation model, which offers good robustness and computational efficiency for transonic airfoil flows. Spatial discretization uses the Roe scheme with the Van Albada flux limiter, and time advancement employs an implicit method assisted by multigrid acceleration techniques.

3.2 Solver and Mesh Strategy

Aerodynamic computations are performed using an in-house developed Computational Fluid Dynamics solver. This solver is based on the finite-volume method and is suitable for unstructured grid systems. Since this solver only supports three-dimensional grids, for airfoil (two-dimensional) aerodynamic analysis, this paper adopts a pseudo-two-dimensional approach: the airfoil section is extruded by one cell thickness along the spanwise direction to generate a three-dimensional grid with a single layer of cells, and symmetry boundary conditions are imposed to simulate infinite-span flow.

Airfoil mesh: An O-topology is used, generated by Pointwise. The total number of mesh cells is approximately 1.7×10^5, and the first-layer grid height is set to 1.0×10^{-5} (dimensionless), ensuring $y+\leqslant1$ at the wall and satisfying the resolution requirement of the S–A model for the viscous sublayer.

Full BWB aircraft mesh: An unstructured grid is used, also generated by Pointwise. The total number of mesh cells is approximately 9.8×10^7, and the first-layer grid height is 0.01 (dimensionless). To accurately capture the complex flow in the fuselage/inboard-wing blending region, anisotropic refinement is applied in regions such as the blending area, leading edge, and trailing edge. The far-field boundary is placed at a sufficient distance to minimize reflection interference.

3.3 Computational *Conditions and Physical Properties*

The computational conditions for airfoil optimization and full aircraft verification are set as follows: freestream Mach number Ma = 0.3266, Reynolds number Re = 3.85468×10^6 (characteristic length =

1 m), and static temperature T = 242.7 K. The molecular Prandtl number is P_r = 0.72, and the turbulent Prandtl number is P_{rt} = 0.9. The pseudo-2D structured mesh for the airfoil and the unstructured mesh for the full BWB aircraft are shown below:

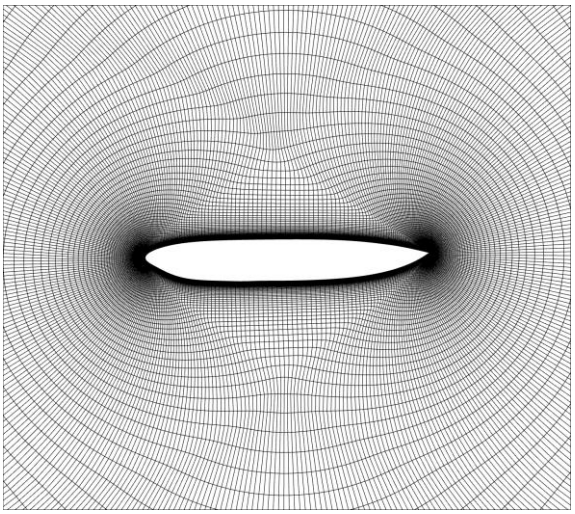


Figure 10 – Schematic of the 2D airfoil mesh

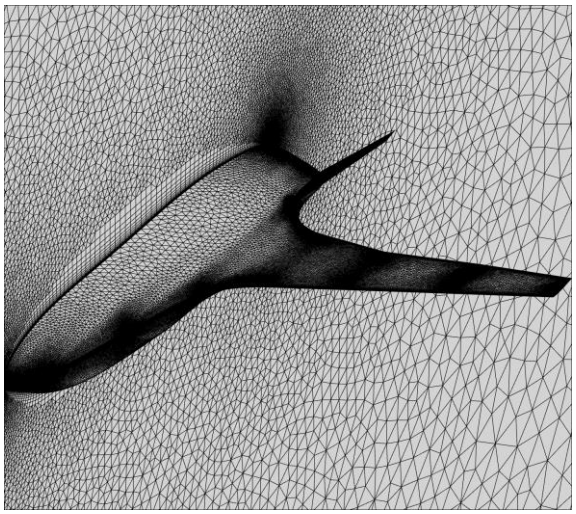


Figure 11 – Schematic of the full BWB aircraft mesh

4. Construction Method of the Comprehensive Airfoil Performance Index W_{01}

To comprehensively evaluate the lift, drag, and pitching moment characteristics in airfoil optimization design, this paper constructs a dimensionless comprehensive index $W_{01} \in [0,1]$, where a larger value indicates better overall airfoil performance. This index is based on the aerodynamic data at the design angles of attack $\alpha = 4°$ and $6°$. By transforming the moment coefficient with the aerodynamic center as the moment reference point, performing statistical standardization, and applying weighted synthesis, the influence of angle of attack is eliminated and the design emphasis can be flexibly reflected.

4.1 Aerodynamic Center and Constant Moment Coefficient

The pitching moment coefficient C_m in the original data is given about the leading edge (reference point $X_{ref} = 0$, chord length $c = 1$) and varies with the lift coefficient. To obtain moment characteristics independent of the angle of attack, it is necessary to determine the aerodynamic center position X_{ac} and the constant moment coefficient $C_{m,ac}$ about this point.

From the aerodynamic relationship, the moment coefficient about the leading edge can be expressed as:

$$C_m(\alpha) = C_{m,ac} - x_{ac} \cdot C_l(\alpha) \tag{9}$$

Using the data at the two design angles of attack $\alpha_1 = 4°$ and $\alpha_2 = 6°$, a system of equations is formed:

$$\begin{cases} C_m(\alpha_1) = C_{m,ac} - x_{ac} \cdot C_l(\alpha_1) \\ C_m(\alpha_2) = C_{m,ac} - x_{ac} \cdot C_l(\alpha_2) \end{cases} \tag{10}$$

By eliminating $C_{m,ac}$, the relative position of the aerodynamic center is obtained:

$$x_{ac} = \frac{C_{my}(\alpha_1) - C_{my}(\alpha_2)}{C_l(\alpha_2) - C_l(\alpha_1)} \tag{11}$$

Then the constant moment coefficient is obtained:

$$C_{m,ac} = C_m(\alpha_1) + x_{ac} \cdot C_l(\alpha_1) \tag{12}$$

The evaluation index for the moment characteristic is taken as the absolute value $|C_{m,ac}|$, where a smaller value indicates a lower trim drag penalty and therefore better performance.

4.2 Representative Aerodynamic Values at Design Points

To improve optimization robustness, the average values at the two design angles of attack are taken as the representative lift and drag values for the airfoil:

$$\bar{C}_l = \frac{C_l(4^\circ) + C_l(6^\circ)}{2}, \quad \bar{C}_d = \frac{C_d(4^\circ) + C_d(6^\circ)}{2} \tag{13}$$

Index Normalization Based on Statistical Standardization. To eliminate dimensional differences and map the values to the interval $[0,1]$, the mean μ and standard deviation σ are calculated for C_l, C_d, and $|C_{m,ac}|$ of all candidate airfoils, and the standard normal cumulative distribution function $\Phi(\cdot)$ is used for score transformation.

Lift coefficient (the larger the better):

$$S_{C_l} = \Phi\left(\frac{\bar{C}_l - \mu_{\bar{C}_l}}{\sigma_{\bar{C}_l}}\right) \tag{14}$$

Drag coefficient (the smaller the better):

$$S_{C_d} = \Phi\left(\frac{\mu_{\bar{C}_d} - \bar{C}_d}{\sigma_{\bar{C}_d}}\right) \tag{15}$$

Absolute moment value (the smaller the better):

$$S_{C_m} = \Phi\left(\frac{\mu_{|C_{m,ac}|} - |C_{m,ac}|}{\sigma_{|C_{m,ac}|}}\right) \tag{16}$$

where $\Phi(z) = \frac{1}{2}[1 + erf(\frac{z}{2})]$

When a certain index equals the population mean, the score is 0.5; the more it exceeds the mean, the closer the score is to 1, and vice versa.

4.3 Weighted Comprehensive Index W_{01}

The comprehensive evaluation index is defined as the weighted sum of the three scores:

$$W_{01} = \lambda_1 S_{C_l} + \lambda_2 S_{C_d} + \lambda_3 S_{C_m} \tag{17}$$

The weight coefficients satisfy $\lambda_1 + \lambda_2 + \lambda_3 = 1$, and $\lambda_i \geq 0$. By adjusting the weights, the optimization direction can be flexibly controlled: increasing λ_1 favors lift, increasing λ_2 favors low drag, and increasing λ_3 emphasizes moment characteristics. This index naturally satisfies $0 \leq W_{01} \leq 1$, and an airfoil with a larger W_{01} has better overall performance.

4.4 Weight Configuration and Airfoil Optimization

In this paper, based on the perturbation CST method, multiple sets of airfoil samples are generated, and the aerodynamic data of each sample are obtained through RANS solutions. With the weights $\lambda = [0.45, 0.5, 0.05]$, the calculated comprehensive ranking is shown in the table below. Among them, the row marked in red and bold: the selected optimized airfoil, to be used for subsequent airfoil assembly and topological design of the fuselage and inboard wing sections; the rows in bold: the baseline airfoils.

Table 1 – Comprehensive Index Ranking of the BYW01 Airfoil Family (y = 0 mm)

Airfoil	Average C_l	Average C_d	$\lvert C_{m,ac}\rvert$	Lift Score	Drag Score	Moment Score	W_{01}
3	**0.1654**	**0.01362**	**0.05639**	**0.4742**	**0.6672**	**0.4762**	**0.5708**
6	0.1681	0.01365	0.06568	0.5496	0.6265	0.1578	0.5684
10	0.1681	0.01368	0.05765	0.5501	0.5908	0.4255	0.5642
16	0.1679	0.01366	0.06394	0.5421	0.6185	0.2044	0.5634
8	0.1637	0.01366	0.04588	0.4266	0.6197	0.8432	0.5440
2	0.1649	0.01364	0.06308	0.4599	0.6412	0.2299	0.5391

15	0.1778	0.01393	0.05099	0.7886	0.2918	0.6874	0.5351
13	0.1456	0.01321	0.05799	0.0734	0.9551	0.4122	0.5312
5	0.1594	0.01359	0.05823	0.3146	0.6964	0.4028	0.5099
19	**0.2049**	**0.01453**	**0.03519**	**0.9965**	**0.0075**	**0.9818**	**0.5013**
18	0.1901	0.01430	0.03195	0.9518	0.0455	0.9923	0.5006
9	0.1672	0.01378	0.06149	0.5237	0.4668	0.2819	0.4832
17	0.1476	0.01344	0.06677	0.0950	0.8337	0.1328	0.4663
12	0.1746	0.01401	0.04862	0.7173	0.2096	0.7671	0.4659
1	0.1766	0.01406	0.04978	0.7643	0.1689	0.7295	0.4649
7	0.1549	0.01360	0.07116	0.2114	0.6809	0.0595	0.4385
4	0.1618	0.01386	0.05403	0.3751	0.3774	0.5715	0.3861
14	0.1404	0.01365	0.05939	0.0347	0.6342	0.3578	0.3506
11	0.1695	0.01417	0.06544	0.5874	0.0958	0.1638	0.3204

Table 2 – Comprehensive Index Ranking of the BYW02 Airfoil Family (y = 650 mm)

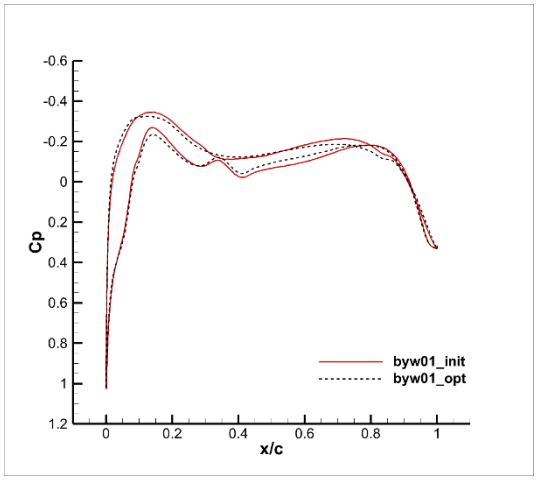
Airfoil	Average C_l	Average C_d	$\lvert C_{m,ac} \rvert$	Lift Score	Drag Score	Moment Score	W_{0l}
12	**0.1676**	**0.01348**	**0.05143**	**0.4870**	**0.6649**	**0.4798**	**0.5756**
16	0.1751	0.01361	0.05393	0.6533	0.5149	0.3622	0.5696
1	0.1688	0.01353	0.04589	0.5142	0.6015	0.7324	0.5688
2	0.1827	0.01376	0.05375	0.7968	0.3450	0.3703	0.5496
19	**0.2016**	**0.01401**	**0.03781**	**0.9722**	**0.1275**	**0.9449**	**0.5485**
9	0.1787	0.01375	0.04686	0.7272	0.3492	0.6924	0.5364
8	0.1621	0.01343	0.05625	0.3627	0.7091	0.2632	0.5309
3	0.1558	0.01335	0.05099	0.2372	0.7864	0.5012	0.5250
13	0.1940	0.01412	0.04370	0.9307	0.0704	0.8119	0.4946
11	0.1549	0.01338	0.05714	0.2232	0.7595	0.2294	0.4917
10	0.1680	0.01366	0.04269	0.4946	0.4516	0.8431	0.4906
5	0.1421	0.01314	0.07252	0.0666	0.9200	0.0046	0.4902
17	0.1337	0.01312	0.05696	0.0239	0.9302	0.2360	0.4876
15	0.1928	0.01414	0.04428	0.9208	0.0639	0.7926	0.4859
18	0.1681	0.01364	0.06370	0.4983	0.4821	0.0624	0.4684
4	0.1855	0.01431	0.03811	0.8388	0.0218	0.9408	0.4354
7	0.1635	0.01371	0.04905	0.3931	0.3937	0.5940	0.4034
14	0.1445	0.01347	0.05257	0.0868	0.6733	0.4253	0.3969
6	0.1740	0.01396	0.05750	0.6293	0.1616	0.2164	0.3748

Table 3 – Comprehensive Index Ranking of the BYW03 Airfoil Family (y = 1200 mm)

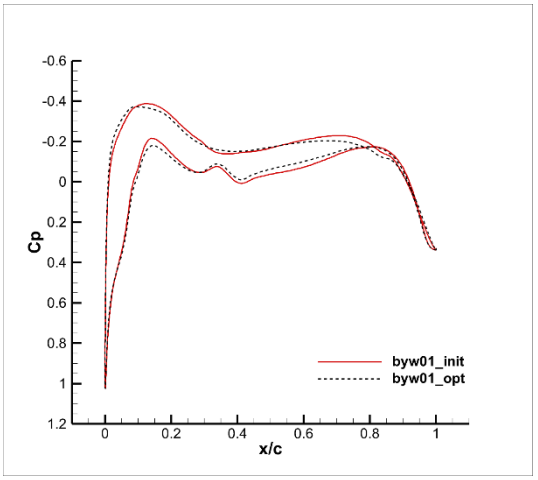
Airfoil	Average C_l	Average C_d	$\lvert C_{m,ac} \rvert$	Lift Score	Drag Score	Moment Score	W_{0l}
10	**0.3719**	**0.01762**	**0.00243**	**0.5328**	**0.5429**	**0.7712**	**0.5498**
11	0.3760	0.01779	0.00027	0.6201	0.4347	0.8809	0.5404
4	0.3548	0.01713	0.00098	0.2003	0.8136	0.8499	0.5394
8	0.3582	0.01707	0.01335	0.2564	0.8367	0.0712	0.5373
7	0.3802	0.01788	0.00513	0.7028	0.3820	0.5779	0.5361
14	0.3494	0.01699	0.00086	0.1297	0.8673	0.8558	0.5348
17	0.3819	0.01798	0.00159	0.7329	0.3226	0.8193	0.5321
9	0.3604	0.01735	0.00183	0.2956	0.7032	0.8064	0.5249
2	0.3768	0.01787	0.00117	0.6373	0.3839	0.8409	0.5208
12	0.3668	0.01753	0.00596	0.4248	0.5979	0.5118	0.5157
5	0.3481	0.01694	0.00850	0.1150	0.8849	0.3139	0.5099
16	0.3293	0.01638	0.00983	0.0133	0.9814	0.2256	0.5080
6	0.3627	0.01750	0.00389	0.3405	0.6185	0.6729	0.4961
1	0.4076	0.01901	0.00235	0.9778	0.0173	0.7765	0.4875
13	0.3563	0.01726	0.01063	0.2245	0.7510	0.1796	0.4855

18	0.3779	0.01804	0.00155	0.6576	0.2850	0.8218	0.4795
15	0.3929	0.01844	0.00977	0.8882	0.1150	0.2288	0.4686
19	**0.4013**	**0.01867**	**0.01683**	**0.9527**	**0.0576**	**0.0150**	**0.4583**
3	0.3865	0.01834	0.00848	0.8078	0.1499	0.3152	0.4542

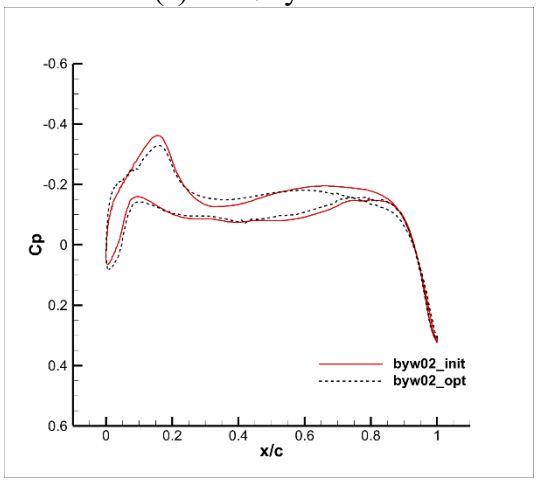
To verify the rationality of using the index based on 2D aerodynamic performance for 3D modeling optimization, byw01 was assembled at y = 0 mm, byw02 at y = 650 mm, and byw03 at y = 1200 mm. The pressure distribution comparison at each section between the optimized configuration BY_opt and the baseline configuration BY_init is shown in the figure below. Combined with the comprehensive index ranking, it can be seen that the lift of the baseline airfoils is almost always higher than that of the optimized airfoils, but the optimized airfoils improve the lift distribution and reduce the absolute value of the pitching moment or drag. Subsequent 3D numerical simulation results show that the overall aircraft performance is improved, with the lift-to-drag ratio, pitching moment, and trim point all being improved to varying degrees. Since this is a synergistic optimization of the fuselage and inboard wing sections, an increase in lift alone does not effectively improve the overall performance; the improvement of the airfoil's comprehensive capability is more important for enhancing the overall performance. This method can effectively distinguish the merits of airfoils, is independent of the baseline airfoil, and has good generality.



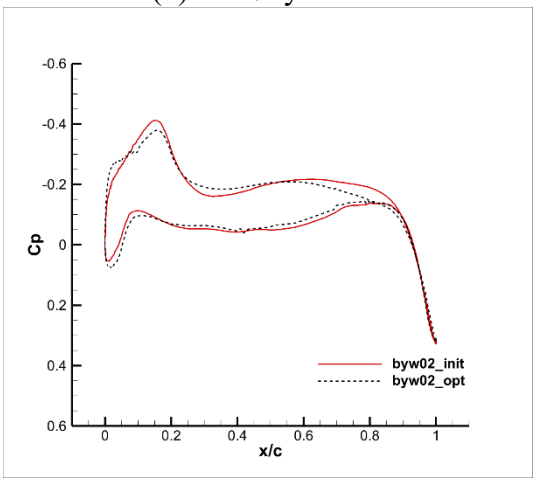
(a)α=4°，y=0mm



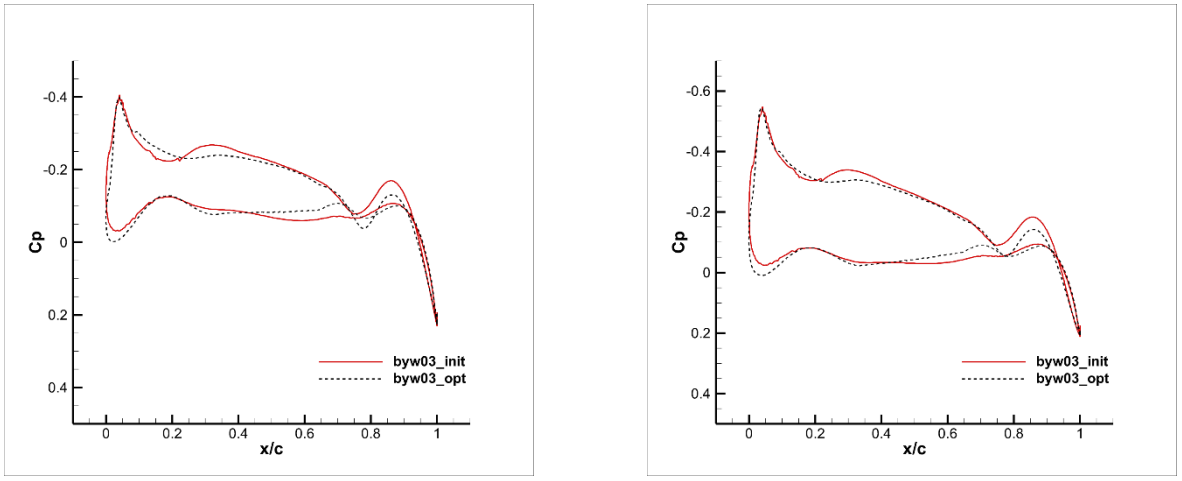
(b)α=6°，y=0mm



(c)α=4°，y=650mm



(d)α=6°，y=650mm



(e)α=4°， y=1200mm　　(f)α=6°， y=1200mm

Figure 12 – Comparison of pressure distribution at different sections of the full BWB aircraft

5. Three-Dimensional Parametric Modeling

Based on the two-dimensional CST parameterization results, this paper carries out the generation and high-fidelity modeling of the three-dimensional shape of the BWB inboard wing section. The specific process is as follows:

5.1 Control Line Interpolation

The leading-edge control line and the trailing-edge control line are given in the form of discrete point sets $\{(x_k^{LE}, y_k^{LE}, z_k^{LE})\}$ and $\{(x_k^{TE}, y_k^{TE}, z_k^{TE})\}$, respectively. For any spanwise coordinate y, the coordinates of the target leading-edge point P_{LE} and the target upper trailing-edge point $P_{TE,u}$ are obtained by linear interpolation. Assuming y falls within the interval $[y_a, y_b]$, the interpolation formula is:

$$\begin{aligned} \lambda &= \frac{y - y_a}{y_b - y_a} \\ x_{\mathrm{LE}}(y) &= (1-\lambda)x_a^{\mathrm{LE}} + \lambda x_b^{\mathrm{LE}} \\ z_{\mathrm{LE}}(y) &= (1-\lambda)z_a^{\mathrm{LE}} + \lambda z_b^{\mathrm{LE}} \end{aligned} \tag{18}$$

Similarly, $x_{TE}(y)$ and $z_{TE}(y)$ can be obtained as the coordinates of $P_{TE,u}$. When y exceeds the range of the control line, the value of the nearest endpoint is taken for extrapolation.

5.2 Airfoil Coordinate Reading and Upper/Lower Surface Separation

The normalized airfoil coordinate file (Selig format) is read in, obtaining the sequence $P = \{(x_i, z_i)\}_{i=1}^{N}$, which starts from the upper surface trailing edge, passes through the leading edge, and reaches the lower surface trailing edge. The index $i_{LE} = \arg\min_i x_i$ of the leading edge point is found to divide the airfoil into the upper surface point set U and the lower surface point set L:

$$\begin{aligned} U &= \{(x_i, z_i) \mid i = 1, 2, \ldots, i_{LE}\}, \\ L &= \{(x_i, z_i) \mid i = i_{LE}, i_{LE}+1, \ldots, N\}. \end{aligned} \tag{19}$$

where the order of U is from the trailing edge to the leading edge, and the order of L is from the leading edge to the trailing edge. The leading edge point is $P_{\mathrm{LE}}^{\mathrm{norm}} = (x_{i_{LE}}, z_{i_{LE}})$, and the upper surface trailing edge point is $P_{\mathrm{TE,u}}^{\mathrm{norm}} = (x_1, z_1)$.

5.3 2D Similarity Transformation

Define the transformation T from the normalized airfoil coordinate system (x, z) to the global coordinate system (X, Z), mapping the normalized leading edge point $P_{LE,u}^{norm}$ to $P_{LE,u}$, and the

normalized upper trailing edge point $P_{TE,u}^{norm}$ to $P_{TE,u}$. This transformation is a similarity transformation involving rotation, uniform scaling, and translation:

$$\begin{pmatrix} X \\ Z \end{pmatrix} = s \begin{pmatrix} \cos\theta & -\sin\theta \\ \sin\theta & \cos\theta \end{pmatrix} \begin{pmatrix} x \\ z \end{pmatrix} + \begin{pmatrix} t_X \\ t_Z \end{pmatrix} \tag{20}$$

The parameters are determined by the two control point pairs. Let the vectors be $\mathbf{v}_1 = P_{TE,u}^{norm} - P_{LE}^{norm}$ and $\mathbf{v}_2 = P_{\mathrm{TE},u} - P_{\mathrm{LE}}$; then the scaling factor is $s = \frac{\|\mathbf{v}_2\|}{\|\mathbf{v}_1\|}$, and the rotation angle is $\theta = \angle(\mathbf{v}_2) - \angle(\mathbf{v}_1)$. The translation vector is:

$$\begin{pmatrix} t_X \\ t_Z \end{pmatrix} = P_{\mathrm{LE}} - s \begin{pmatrix} \cos\theta & -\sin\theta \\ \sin\theta & \cos\theta \end{pmatrix} P_{\mathrm{LE}}^{\mathrm{norm}} \tag{21}$$

Apply T to all airfoil points to obtain the assembled coordinates $\tilde{P}_i = T\left(P_i^{norm}\right)$.

5.4 Trailing Edge Thickness Adjustment

According to the specified trailing edge thickness t_{TE} (global dimension), the target lower trailing edge point $P_{TE,l}$ is obtained by shifting the upper trailing edge point downward in the Z direction:

$$P_{TE,l} = (x_{TE}(y), z_{TE}(y) - t_{TE}) \tag{22}$$

After the similarity transformation, the current coordinate of the lower surface trailing edge point is $\tilde{P}_{TE,l}^{cur} = T(P_{TE,l}^{norm})$. To make it coincide with the target point $P_{TE,l}$, a smooth offset gradually varying from the leading edge to the trailing edge is applied to all lower surface points. Define the chordwise parameter r for each lower surface point:

$$r = \frac{X_{\mathrm{TE},u} - X}{\| P_{\mathrm{TE},u} - P_{\mathrm{LE}} \|} \tag{23}$$

where $X_{TE,u}$ is the X coordinate of the upper trailing edge. Then the corrected lower surface coordinates are:

$$\begin{aligned} \Delta Z &= z_{\mathrm{TE},l} - \tilde{z}_{\mathrm{TE},l}^{\mathrm{cur}} \\ Z_i^{\mathrm{final}} &= \tilde{z}_i + \Delta Z \cdot r, \quad \forall \tilde{P}_i \in \tilde{L}, i > 0 \end{aligned} \tag{24}$$

The leading edge point ($r=0$) remains unchanged, the trailing edge point ($r=1$) receives the full offset ΔZ, and the intermediate points transition linearly.

5.5 3D Coordinate Synthesis and Output

The upper surface points and the corrected lower surface points are merged in Selig order (upper surface trailing edge → leading edge, lower surface point after leading edge → trailing edge), and the spanwise coordinate $Y = y$ is added to form the final 3D airfoil section point set: $\{(X_i^{final}, y, Z_i^{final})\}$. All assembled sections are written to a file, with the first line being the number of points and each subsequent line containing three floating-point numbers. Simultaneously, the leading-edge control line, the upper trailing-edge control line, and the lower trailing-edge control line file generated by shifting the entire $P_{TE,u}$ downward are output for subsequent geometric modeling.

Finally, the entire set of associated parameters (control line point coordinates) is used as input to drive the geometric kernel of the parametric modeling software CATIA. By invoking high-order spline surface generation algorithms, smooth fitting and lofting are performed on the discrete section curves and boundary lines, ultimately generating a 3D model of the BWB fuselage and inboard wing section with a continuous surface and smooth curvature.

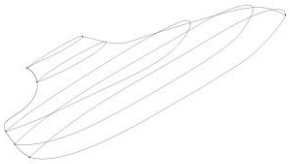


Figure 13 – Schematic of curve fitting and lofting



Figure 14 – Fuselage and inboard wing section model

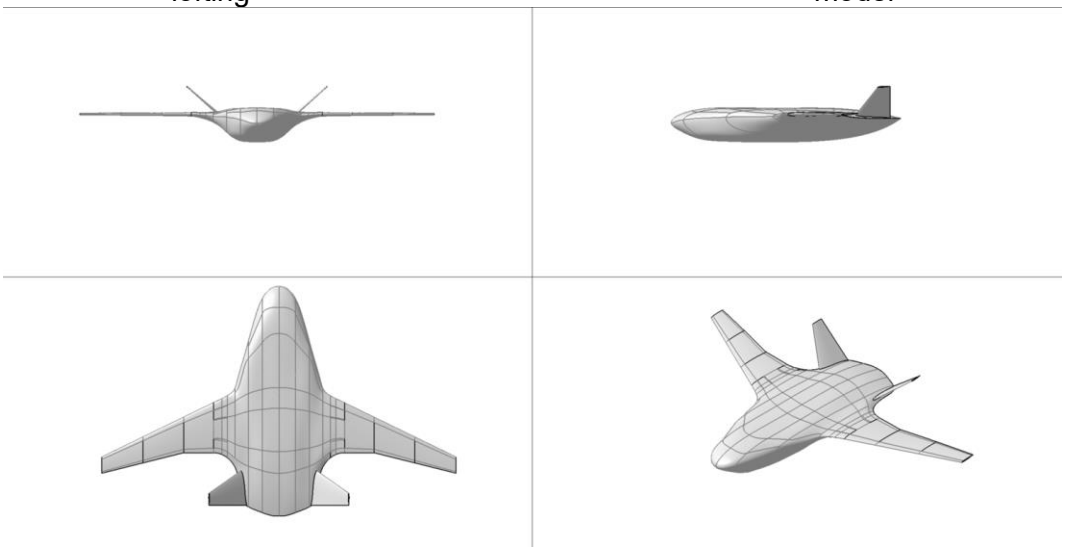


Figure 15 – Multi-view of the full aircraft model

This modeling method achieves a direct and rapid transformation from a small number of design variables to a complex 3D shape. The resulting model not only has high geometric accuracy but also fully meets the model quality requirements for subsequent computational fluid dynamics (CFD) mesh generation, laying a solid geometric foundation for the next step of multi-objective optimization iterations.

6. Multi-objective Optimization and Results

Based on the 3D parametric modeling, a multi-objective optimization framework centered on aerodynamic and moment characteristics is constructed. This paper presents a comparison of various indicators between the final optimized configuration BY_opt and the baseline configuration BY_init, with the following objectives:

Objective 1 (Three-in-One): Through shape modification, while satisfying the cruise design lift coefficient, reduce the pitching moment trim penalty at the state of maximum lift-to-drag ratio, and improve the overall efficiency at the design point.

Objective 2 (Inflection Point Delay): While maintaining the lift-to-drag ratio without degradation, delay the wing root separation by optimizing the chordwise pressure distribution and section camber/twist in the swept region, achieving a rearward shift of the pitching moment curve inflection point to a higher angle of attack, thereby expanding the stable flight envelope.

Optimization Results:

(1) Under cruise conditions, the lift-to-drag ratio increases by 4.72%, and the absolute value of the pitching moment decreases by 15.44%;

(2) The angle of attack corresponding to the inflection point of the pitching moment curve is shifted rearward by 0.36° compared to the baseline configuration, an improvement of 3.62%.

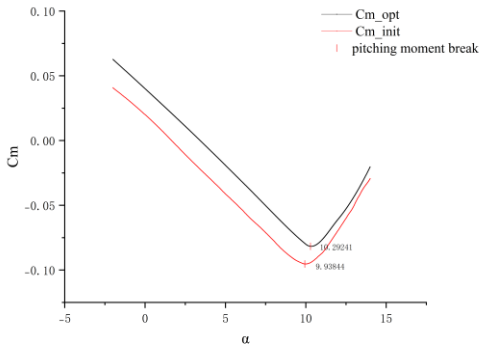


Figure 16 – Comparison of Cm-α curves

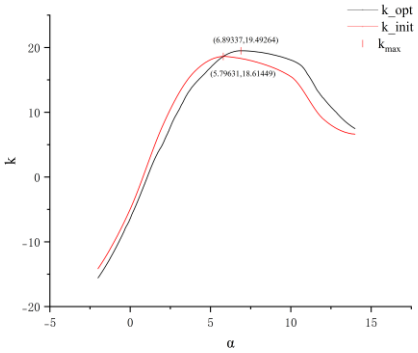


Figure 17 – Comparison of k-α curves

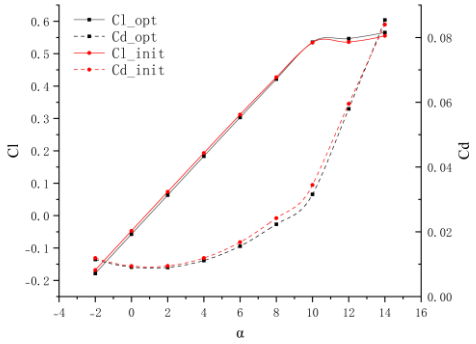
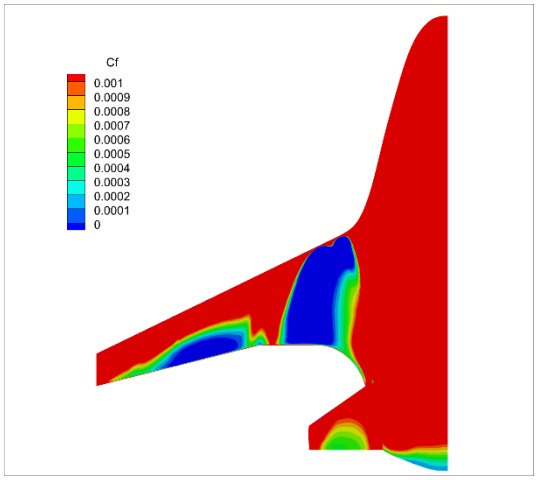


Figure 18 – Comparison of Cl-Cd-α curves

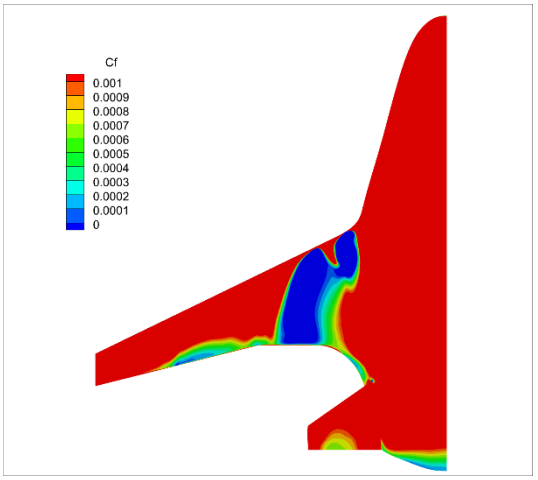
Table 4 – Comparison of optimization indicators

Name	BY_init	BY_opt	Δ	Improvement rate
k_{max}	18.614	19.492	0.878	4.72%
angle of attack at the pitching moment break	9.938°	10.292°	0.36°	3.62%
pitching moment coefficient at k_{max}	-0.0505	-0.0427	0.0078	15.44%
Cl at k_{max}	0.2996	0.3564	/	/
Cd at k_{max}	0.01638	0.01842	/	/

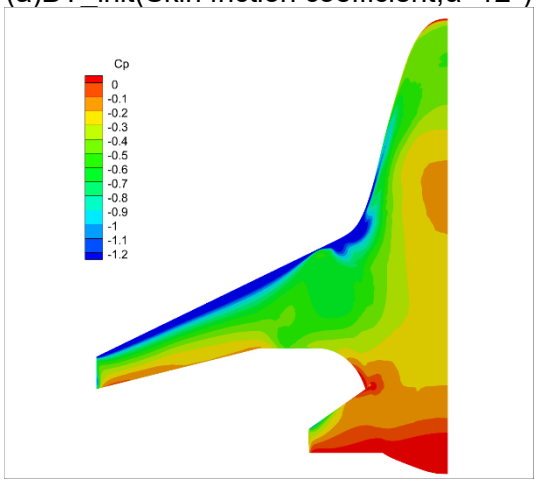
The surface flow field information of the two configurations at an angle of attack of 12° was extracted for analysis. The skin friction distribution comparison between the optimized configuration and the baseline configuration is shown in Figs. 18(a) and 18(b), the pressure distribution comparison is shown in Figs. 18(c) and 18(d), and the spatial and surface limiting streamline comparison is shown in Figs. 19(a) and 19(b). The comprehensive analysis reveals that the optimized configuration confines the separation zone in the blending region to the leading edge, forming a small separation bubble and weakening the vortices at the wing root, so that the separation zone does not expand onto the wing. From the surface limiting streamlines on the wing, it is clearly observed that the spanwise velocity at the wing root of the optimized configuration expands only slightly onto the wing. As a result, flow separation on the wing is delayed, the inflection point of the pitching moment curve is shifted rearward, and the lift-to-drag ratio is improved.



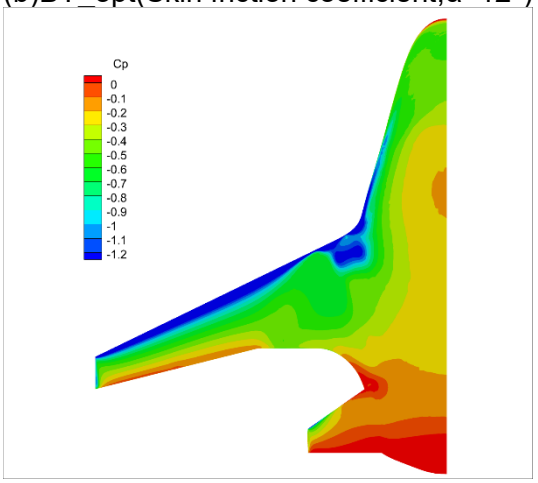
(a)BY_init(Skin friction coefficient,α=12°)



(b)BY_opt(Skin friction coefficient,α=12°)

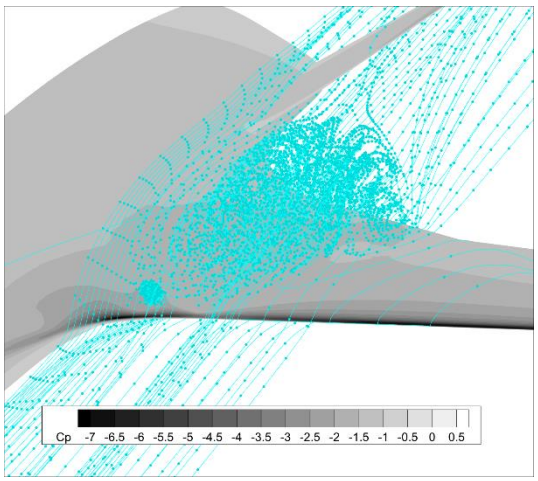


(c) BY_init (Pressure coefficient, α=12°)

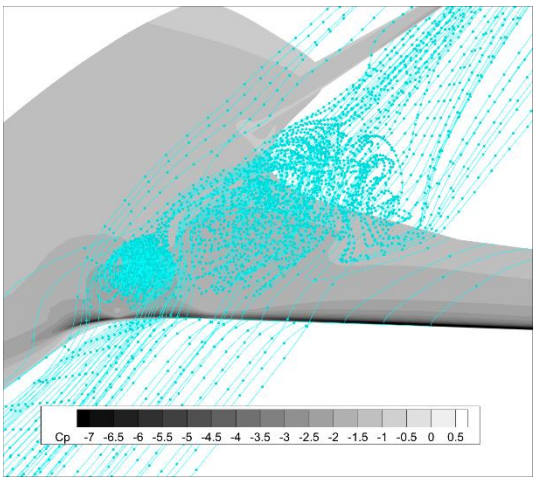


(d) BY_opt (Pressure coefficient, α=12°)

Figure 18 – Comparison of surface flow field information



(a)BY_init(α=12°)



(b)BY_opt(α=12°)

Figure 19 – Comparison of streamlines

7. Conclusions

Aiming at the aerodynamic coupling problem of the fuselage and inboard wing sections of a BWB aircraft, this paper proposes an airfoil reconstruction method based on perturbation CST

parameterization and multi-objective optimization. The following conclusions are drawn:

(1) The proposed perturbation CST parameterization method combines geometric shape preservation with design freedom, maintaining the basic aerodynamic characteristics of the baseline airfoil within a local perturbation range. The fitting accuracy of the airfoils at each characteristic section is controlled within 0.7%, verifying the effectiveness of the CST method in parameterizing the airfoils of the BWB blending region.

(2) The constructed comprehensive airfoil evaluation index W_{01} is based on aerodynamic center transfer and statistical standardization techniques, integrating lift, drag, and the constant pitching moment coefficient about the aerodynamic center. Through weight configuration ($\lambda_1=0.45$, $\lambda_2=0.50$, $\lambda_3=0.05$), quantitative ranking of candidate airfoils is achieved, and the optimized airfoil with the best overall performance at each section is successfully selected.

(3) A complete parametric modeling workflow from 2D airfoil optimization to 3D geometric assembly is established. By means of control line interpolation, similarity transformation, and gradual trailing edge thickness adjustment, the optimized airfoils are assembled into 3D space, generating a high-fidelity model of the BWB blending region lofted with high-order spline surfaces, which provides a high-quality geometric basis for CFD analysis.

(4) The full aircraft numerical simulation results show that, under the design condition, the optimized configuration achieves a 4.72% increase in lift-to-drag ratio, a 7.3% reduction in drag coefficient, a 15.44% rearward shift of the pitching moment curve inflection point, and a 15.44% decrease in the absolute value of the pitching moment at the cruise point compared with the baseline configuration. The Q-criterion vortex structure analysis indicates that the optimized configuration effectively suppresses the development of the wing-root separation zone and forms a small separation bubble that is conducive to delaying separation, thereby achieving a synergistic improvement in both moment characteristics and lift-to-drag characteristics.

References

[1] Sun Y., Wang C., Li R. et al. Review on the Development of Blended-Wing-Body Configuration Civil Aircraft: History, Progress and Prospect. *Lecture Notes in Mechanical Engineering*, pp 387-412, 2025.

[2] Ouyang T., Chen J., Liu D. et al. Current Development and Revelation of Blended-Wing-Body Aircraft. *Lecture Notes in Mechanical Engineering*, pp 105-118, 2025.

[3] Wang L., Zhang N., Liu H. et al. Stability characteristics and airworthiness requirements of blended wing body aircraft with podded engines. *Chinese Journal of Aeronautics*, Vol. 35, No. 6, pp 77-86, 2022.

[4] Yu M., Tao Z., Li H. et al. Optimizing the Landing Stability of Blended-Wing-Body Aircraft with Distributed Electric Boundary-Layer Ingestion Propulsors through a Novel Thrust Control Configuration. *Applied Sciences (Switzerland)*, Vol. 14, No. 18, 8546, 2024.

[5] Mody P. C., Sato S., Hall D.K. et al. Conceptual design of an N+3 hybrid wing body subsonic transport. Vol. 1, 2010.

[6] Nickol C. L. and McCullers L. A. Hybrid Wing body configuration system studies. 2009.

[7] Okonkwo P. and Smith H. Review of evolving trends in blended wing body aircraft design. *Progress in Aerospace Sciences*, Vol. 82, pp 1–23, 2016.

[8] Wang G., Zhang B., Zhang M. et al. Research progress and prospect for conceptual and aerodynamic technology of blended-wing-body civil aircraft. *Hangkong Xuebao/Acta Aeronautica et Astronautica Sinica*, Vol. 40, No. 9, 2019.

[9] Ali U., Okasha M., Dief T. N. et al. A. Blended wing body designs for aerodynamic, stability, and control optimization: A comprehensive review. *Transportation Engineering*, Vol. 22, 2025.

[10] Nadzari M. N. I. B. M., Muta'ali A. B. A. and Nasir R. E. B. M. Multi-Disciplinary Optimisation (MDO) of a Blended Wing-Body (BWB) Aeroplane Design with Variable Wing Sweep Angle. *Journal of Aeronautics, Astronautics and Aviation*, Vol. 57, No. 3, pp 341-353, 2025.

[11] Zhang M., Rizzi A., Meng P. et al. Aerodynamic design considerations and shape optimization of flying wings in

transonic flight. Proc *12th AIAA Aviation Technol. Integr. Oper. (ATIO) Conf. 14th AIAA/ISSMO Multidiscip. Anal. Optim. Conf.*, 2012.

[12]Cui Y., He J., Li Q. et al. Multi-Point Optimization Design of Blended Wing Body Based on Discrete Adjoint Method. *Aerospace*, Vol. 12, No. 5, 2025.

[13]Yazdi R R S, Gray A L and Zingg D W. Optimization of Twin-Aisle-Class Blended-Wing-Body Aircraft Incorporating Critical Requirements and High-Fidelity Aerodynamic Modelling. *AIAA Science and Technology Forum and Exposition, AIAA SciTech Forum 2026*, 2026.

[14]Chan J. L. C., Sun Y. and Smith H. Conceptual designs of blended wing body aircraft for the application of alternative fuels. *AIAA Aviation Forum and ASCEND, 2024*, 2024.

[15]Rasheed R., Jayalingam K., Muthuswamy P. et al. Analysis of changing trends in blended wing body aircraft design. *AIP Conference Proceedings*, Vol. 2937, No. 1, 2024.

[16]Kulfan B. M. A universal parametric geometry representation method - 'CST'. Vol. 1, pp 657–691, 2007.

[17]Lane K. A. and Marshall D. D. A surface parameterization method for airfoil optimization and high lift 2D geometries utilizing the CST methodology. Proc *AIAA Aerosp. Sci. Meet. New Horiz. Forum Aerosp. Expos.*, 2009.

[18]Godfrey A. H. and Nelson C. A Benchmark and Comparison of Airfoil Parameterization and Optimization Techniques. Proc *AIAA Sci. Technol. Forum Expos.*, 2025.

[19]Wang K., Wang W. and Zheng X. Parameterized Modeling of Blended Wing Body AircraftBased on Multi-Scale CST Method. *Aero Weaponry*, Vol. 32, No. 4, pp 120–127, 2025.

[20]Bu Y., Song W., Han Z. et al. Aerodynamic Optimization Design of Airfoil Based on CST Parameterization Method. *Journal of Northwestern Polytechnical University*, Vol. 31, No. 05, pp 829–836, 2013.

[21]Li J., Gao Z., Huang J. et al. Aerodynamic optimization system based on CST technique. *Acta Aerodynamica sinica*, Vol. 30, No. 04, pp 443–449, 2012.

[22]Tang F., Du N., Jiao Z. et al. Optimization of Loitering Missile Airfoils Based on CST Parametric Method. *Journal of Ballistics*, pp 1–9, 2026.

[23]Yin M, He E, Li Y and Zhang C. Aerodynamic shape optimization of hypersonic vehicle based on improved class-shape-transformation method. *Advances in Space Research*, Vol. 76, No. 9, pp 5518-5534, 2025.

[24]Anusonti-Inthra P. Airfoil Parameterization using An Orthogonal Class Shape Transformation. *AIAA SciTech Forum and Exposition*, 2024.

[25]Yang Y, Su H, Gong C, Gu L, Ding X and Wang Z. Analytical aero-structural modeling and optimization method of three-dimensional wing based on CST. *Hangkong Dongli Xuebao/Journal of Aerospace Power*, Vol. 39, No. 4, 2024.

[26]Yan B, Si Y, Zhou Z, Guo W, Wen H and Wang Y. B-spline based on vector extension improved CST parameterization algorithm. *Engineering Reports*, Vol. 6, No. 8, 2024.

Copyright Statement

The authors confirm that they, and/or their company or organization, hold copyright on all of the original material included in this paper. The authors also confirm that they have obtained permission, from the copyright holder of any third party material included in this paper, to publish it as part of their paper. The authors confirm that they give permission, or have obtained permission from the copyright holder of this paper, for the publication and distribution of this paper as part of the ICAS proceedings or as individual off-prints from the proceedings.